THE JOURNAL OF PHYSICAL CHEMISTRY Letters

Letter

pubs.acs.org/JPCL

Inkjet Printing of High Conductivity, Flexible Graphene Patterns

Ethan B. Secor,[†] Pradyumna L. Prabhumirashi,[†] Kanan Puntambekar,[†] Michael L. Geier,[†] and Mark C. Hersam*[,†,‡,§]

[†]Department of Materials Science and Engineering, [‡]Department of Chemistry, and [§]Department of Medicine, Northwestern University, Evanston, Illinois 60208, United States

Supporting Information

ABSTRACT: The ability to print high conductivity, conformal, and flexible electrodes is an important technological challenge in printed electronics, especially for large-area formats with low cost considerations. In this Letter, we demonstrate inkjet-printed, high conductivity graphene patterns that are suitable for flexible electronics. The ink is prepared by solution-phase exfoliation of graphene using an environmentally benign solvent, ethanol, and a stabilizing polymer, ethyl cellulose. The inkjet-printed graphene features attain low resistivity of 4 mΩ·cm after a thermal anneal at 250 °C for 30 min while showing uniform morphology, compatibility with flexible substrates, and excellent tolerance to bending stresses.

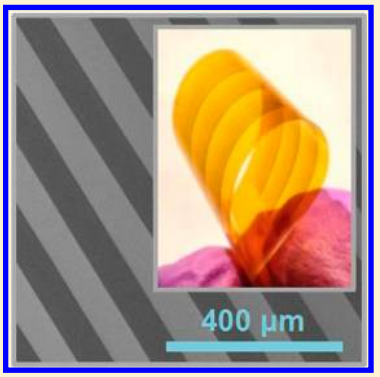

SECTION: Physical Processes in Nanomaterials and Nanostructures

Printed electronics offer an attractive alternative to conventional technologies by enabling low-cost, large-area, flexible devices[1,2] that have the potential to enable unique advances in varied applications such as health diagnostics,[3] energy storage,[4] electronic displays,[5] and food security.[6] Among available manufacturing techniques, inkjet-printing-based fabrication is a promising approach for rapid development and deployment of new material inks. The main advantages of this technology include digital and additive patterning, reduction in material waste, and compatibility with a variety of substrates with different degrees of mechanical flexibility and form factor. Various technologically important active components have been inkjet-printed,[7] including transistors,[8,9] solar cells,[10,11] light-emitting diodes,[12] and sensors.[13,14] Despite these device-level advances, the ability to pattern low-resistance metallic electrodes with fine resolution remains an important challenge, especially as the field evolves toward highly integrated systems.

Graphene is a prominent contender as a metallic component in printed electronic devices due to its high conductivity, chemical stability, and intrinsic flexibility.[15−20] In particular, graphene inks provide an alternative to conventional carbon-based inks that have shown limited conductivity, especially in formulations compatible with inkjet printing.[21] However, such an application requires the production of large-area graphene that can be easily manipulated into complex device architectures. Some of the primary methods that are being explored for the mass production of graphene include growth by chemical vapor deposition (CVD),[22] sublimation of Si from SiC,[23] and solution-phase exfoliation of graphite[24,25] or reduced graphene oxide (RGO).[26−29] Among these approaches, solution-phase exfoliation offers significant advantages such as inexpensive raw materials, the potential for scalability, low thermal budget, and compatibility with additive printing techniques. Exploiting these attributes, previous studies have demonstrated inkjet printing of RGO for organic thin-film transistor electrodes,[30] temperature sensors,[31] radio frequency applications,[32] and chemical sensors.[14] Nevertheless, because the electrical properties of RGO are inferior to those of graphene,[33,34] inkjet printing of pristine graphene flakes is expected to have clear advantages in electronic applications.

Graphene can be directly exfoliated by ultrasonication in select solvents[35] and superacids[36] or through the use of additives such as planar surfactants[37] and stabilizing polymers,[38,39] resulting in relatively small (<10 μm^2 in area) graphene flakes. While small flakes are necessary for stable inkjet printing, they introduce an increased number of flake-to-flake junctions in percolating films, which renders them more resistive compared to CVD-grown or mechanically exfoliated graphene. In addition, traditional solvents and surfactants employed for graphene exfoliation leave persistent residues even following extensive annealing, further disrupting the conductive network.[24,40] Herein, we present a holistic approach for achieving high-performance printed graphene features that addresses the entire process flow starting with graphene exfoliation and proceeding through ink formulation, printing, and final annealing. Central to this approach is the use of graphene exfoliated in the inexpensive, environmentally benign solvent, ethanol, with the stabilizing polymer, ethyl cellulose

Received: March 23, 2013
Accepted: April 8, 2013
Published: April 8, 2013

(EC).[38] Building on this platform, we demonstrate stable inkjet printing of graphene to fabricate high conductivity patterns suitable for flexible electronics.

Graphene inks were produced by the exfoliation of graphite in ethanol and EC, as reported previously.[38] This process primarily produces few-layer graphene sheets, with typical thicknesses of ~2 nm and areas of ~50 × 50 nm^2 (Supporting Information Figure S1). The processing steps are illustrated schematically in Figure 1. In particular, excess graphite and EC

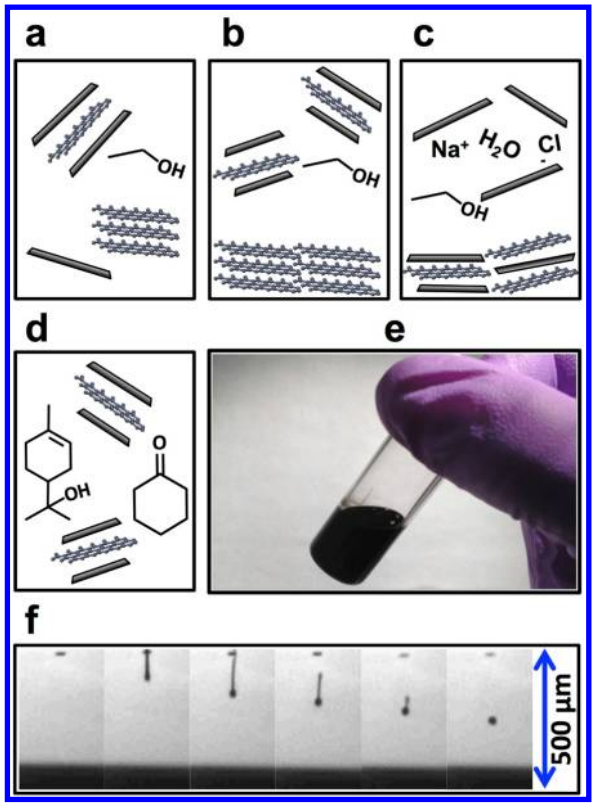

Figure 1. Schematic illustration of the ink preparation method. (a) Graphene is exfoliated from graphite powder in ethanol/EC by probe ultrasonication. A graphene/EC powder is then isolated following (b) centrifugation-based sedimentation to remove residual large graphite flakes and (c) salt-induced flocculation of graphene/EC. (d) An ink for inkjet printing is prepared by dispersion of the graphene/EC powder in 85:15 cyclohexanone/terpineol. (e) Vial of the prepared graphene ink and (f) drop formation sequence for inkjet printing, with spherical drops forming after ~300 μm.

were used to achieve high yields of suspended graphene (>0.1 mg/mL). Sedimentation-based centrifugation was then employed (Figure 1a,b) to remove remaining large graphite flakes, yielding a dispersion of ~1:100 graphene/EC in ethanol. To remove excess EC and solvent, a room-temperature method based on the flocculation of graphene/EC was developed. Specifically, upon the addition of NaCl(aq), a solid containing graphene and EC was flocculated and collected following a short centrifugation step (Figure 1c). This graphene/EC solid was subsequently washed with water and dried, yielding a black powder with a graphene content of ~15% (Supporting Information Figure S2), which is significantly higher than the graphene/EC ratio in the original dispersion. Because EC encapsulates graphene flakes in solution, no irreversible aggregation of graphene was observed. The resulting powder is readily dispersed in a variety of solvents, allowing for the tailoring of inks for a range of deposition methods. In particular, dispersion of this material in select organic solvents (Figure 1d,e) enables deposition of graphene by inkjet printing (Figure 1f).

Inkjet printing requires careful tailoring of the viscosity and surface tension of the ink formulation to achieve stable droplet formation. The wetting and drying properties of the ink must also be tuned to achieve proper morphology of the printed features.[41] Furthermore, inks should not possess large particles or volatile solvents because these components can lead to clogging of the inkjet printhead. Finally, a high concentration of graphene is desired to reduce the number of necessary printing passes. To achieve these goals, the graphene/EC powder was dispersed in an 85:15 mixture of cyclohexanone/terpineol (Figure 1d). At a concentration of 2.4 wt % solids (~3.4 mg/mL graphene), this ink has a surface tension of ~33 mN/m and a high shear rate (100−1000 s^{-1}) viscosity of 10−12 mPa·s at 30 °C (Supporting Information Figure S3).

The relatively low surface tension of this ink is designed for proper wetting of low-surface-energy substrates applicable to flexible electronics. To assess the electrical characteristics of the ink, the well-defined substrate of Si/SiO_2 with 300 nm thermally grown oxide was used. For a more suitable model of wetting and drying on low-surface-energy substrates, the Si/SiO_2 substrate was treated with hexamethyldisilazane (HMDS) to decrease the surface energy. Printing was carried out at 30 °C using a Fujifilm Dimatix Materials Printer (DMP 2800) with a cartridge designed for a 10 pL nominal drop volume. Drop spacing for all printed features was maintained at 20 μm. Stable printing of graphene lines on HMDS-treated Si/SiO_2 yielded a line width of ~60 μm, as shown in Figure 2a−c. The highly uniform dome-shaped cross-sectional profile across the lines provides evidence for successful ink formulation, specifically showing no undesirable coffee ring effects. Importantly, this advantageous cross-sectional profile was maintained after multiple printing passes, as shown in Figure 2d. This excellent morphology of the printed features is attributed to the suppression of the coffee ring effect through a Marangoni flow established by the surface tension gradient that develops due to solvent evaporation.[7,42−45] This flow homogenizes the droplet composition, resulting in a uniform morphology of the printed features. In addition, the sp^2 bonding and small lateral size of the graphene flakes minimize folding or buckling of the printed flakes, which promotes low surface roughness and well-defined flake−flake contacts.

The polymeric binder EC encapsulates graphene flakes following solvent evaporation, necessitating thermal annealing to obtain highly conductive features. To study the electrical behavior of the composite material as a function of annealing conditions, films were blade-coated on glass slides and annealed in an ambient atmosphere with systematic variations in the annealing time and temperature. As shown in Figure 3a, a 250−350 °C anneal for 30 min results in high conductivity graphene films. At 250 °C, annealing for as short as 20 min was sufficient to achieve low resistivity (Figure 3b). For the remainder of this study, an annealing temperature and time of 250 °C and 30 min, respectively, were chosen to enable compatibility with flexible electronics applications.

For a detailed assessment of the electrical performance of the printed features, 4 mm long lines with varying thicknesses were printed on HMDS-treated SiO_2 and annealed at 250 °C for 30 min. The line thickness increases linearly with the number of printed layers, with each layer adding ~14 nm to the thickness

dx.doi.org/10.1021/jz400644c | J. Phys. Chem. Lett. 2013, 4, 1347−1351

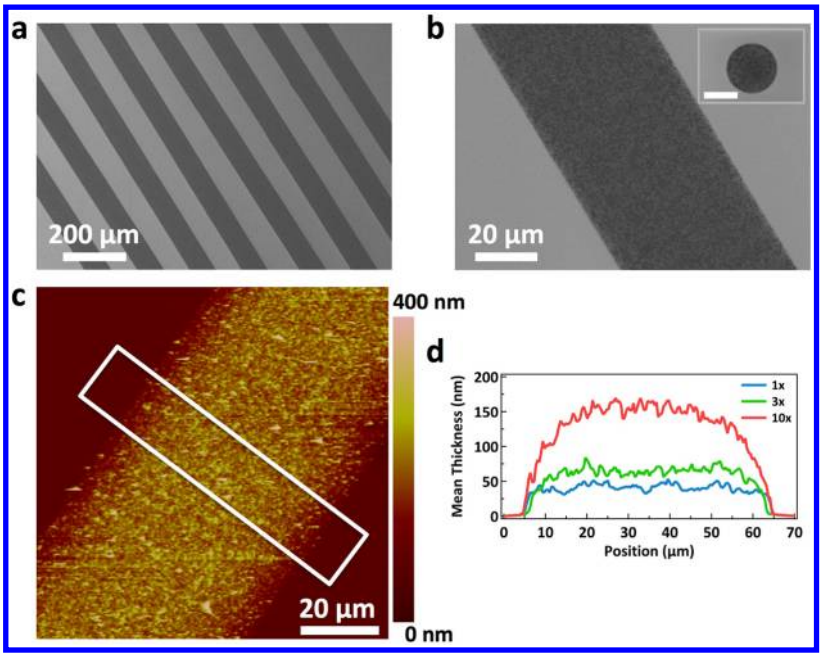

Figure 2. Morphology of inkjet-printed graphene features on HMDS-treated Si/SiO_2. Scanning electron micrographs of (a) multiple printed lines and (b) a single printed line and drop (inset, scale bar corresponds to 40 μm) illustrate the uniformity of the printed features. (c) An atomic force microscopy (AFM) image of a single line following 10 printing passes that shows no coffee ring features. (d) Averaged cross-sectional profiles of printed lines after 1, 3, and 10 printing passes, which demonstrate the reliable increase in thickness obtained after multiple printing passes. The cross-sectional profiles are obtained from the averaged AFM height profile over ~20 μm as indicated by the boxed region in (c).

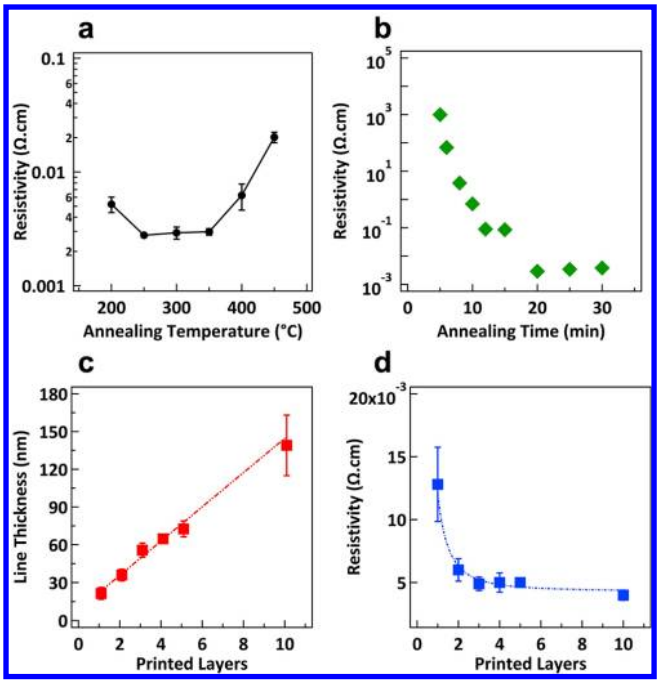

Figure 3. Electrical characterization of graphene features. (a) Electrical resistivity of blade-coated films plotted against the annealing temperature for a fixed annealing time of 30 min, showing effective binder decomposition at 250 °C and increased resistivity due to graphene oxidation above 400 °C. (b) Dependence of electrical resistivity on the annealing time for a fixed annealing temperature of 250 °C, showing that low resistivity is achieved following annealing for 20 min. (c) Thickness of inkjet-printed graphene lines on HMDS-treated Si/SiO_2 for increasing numbers of printing passes. (d) Electrical resistivity of the printed features for increasing numbers of printing passes, showing relatively stable performance after only three printing passes.

(Figure 3d). The line resistivity reaches a relatively stable low value after only three printing passes, owing to the high concentration of the ink and the excellent morphology of the printed features (Figure 3c). The measured conductivity of $2.5 \times 10^4 \pm 0.2 \times 10^4$ S/m (resistivity of $4 \times 10^{-3} \pm 0.4 \times 10^{-3}$ Ω·cm) for the printed lines after 10 printing passes is ~250 times higher than that previously reported for inkjet-printed graphene.[18] This dramatic improvement indicates the effectiveness of the method presented here, which avoids the graphene degradation that occurs in competing processes based on ultrasonication of graphene in harsh solvents.

Thermal gravimetric analysis (TGA) of the ink indicates that EC decomposition occurs in two stages, with a low-temperature charring beginning below 250 °C and volatilization and removal of the EC residue occurring at temperatures above 400 °C (Supporting Information Figure S2). This observation coupled with the high electrical conductivity observed after annealing at temperatures of 250−350 °C suggests that the initial decomposition of EC enables efficient charge transport through the graphene network. Because cellulose derivatives can thermally decompose into aromatic species,[46,47] the resulting $\pi-\pi$ stacking between the residues and the graphene flakes provides relatively efficient charge transport. In addition, the increase in resistivity upon annealing at 400−450 °C correlates well with the removal of residue from the film in the second stage of EC decomposition. Furthermore, the EC residue creates a dense and continuous film, as determined from scanning electron micrographs of printed lines following annealing at 250 and 450 °C (Supporting Information Figure S4). This film densification could potentially enhance the mechanical properties of the printed graphene features and enable a robust tolerance for bending stresses in flexible applications.

To assess mechanical properties, lines were printed on polyimide (DuPont Kapton 125 μm) substrates and annealed

dx.doi.org/10.1021/jz400644c | J. Phys. Chem. Lett. 2013, 4, 1347−1351

at 250 °C for 30 min. Various flexibility tests were employed to characterize these printed graphene lines. For example, to investigate the reliability over a large number of bending cycles, the electrical resistance was measured up to 1000 cycles. As shown in Figure 4a, there is no observable degradation in the

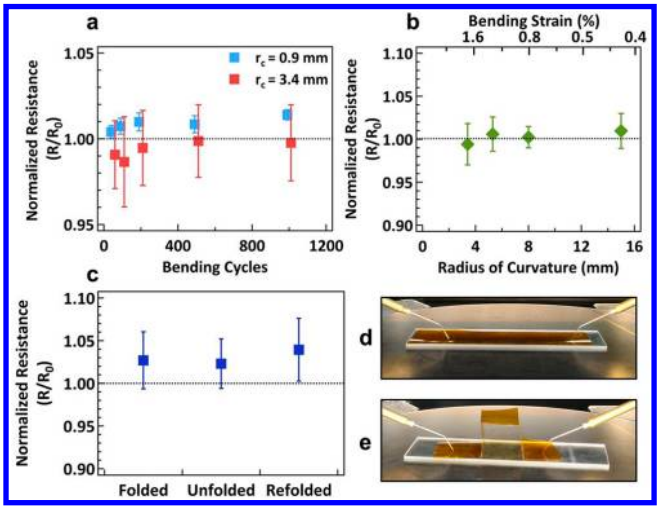

Figure 4. Flexibility assessment of printed graphene lines on kapton substrates. (a) Resistance of graphene lines folded to a radius of curvature of 0.9 mm (blue, bending strain: 6.9%) and 3.4 mm (red, bending strain: 1.8%) normalized to the resistance prior to bending. (b) Normalized resistance of graphene lines measured in a flexed state for various degrees of bending, showing reliable retention of electrical conductivity across all measured flex states. (c) Normalized resistance of graphene lines while measured in a folded state, showing a small and irreversible increase in resistance following folding. Images of the sample in the (d) original and (e) folded state.

line conductivity for a bending radius of curvature of 3.4 mm. Even at a radius of 0.9 mm, the resistance remained nearly unchanged after a marginal initial increase. At this radius of curvature, cracking was observed in the substrate, which suggests that the small loss of conductivity is a limitation of the substrate rather than the printed features. The electrical performance of the printed features was also measured under applied stress for various radii of bending (Figure 4b), with no observed loss in conductivity. As a final test, the resistance of the graphene lines was measured in a folded state, as shown in Figure 4c–e, again resulting in only a slight decrease in conductivity on the order of 5% that can again likely be attributed to substrate cracking. Overall, these mechanical tests show the utility of our graphene inks in flexible, and possibly even foldable, electronic applications.

In summary, we have developed a novel graphene ink based on a graphene/EC powder that is produced using only room-temperature processing methods. The graphene/EC powder allows for careful tuning of the ink to achieve stable inkjet printing of features on a variety of substrates with excellent morphology and could, in principle, be applied to other printing techniques in a straightforward manner. In addition, the conductivity of printed features following mild annealing is over 2 orders of magnitude better than that previously reported for inkjet-printed graphene despite a smaller flake size, thus indicating efficient flake–flake charge transport. We believe that these results are enabled by the synergistic EC binder for graphene exfoliation, which reduces flake–flake junction resistance upon annealing relative to that of graphene films containing residual solvent or surfactant. Finally, the low processing temperatures enable compatibility with flexible substrates, thereby allowing demonstration of the high tolerance of printed graphene features to bending stresses. With this unique combination of attributes, these graphene-based inks are likely to find utility in a wide range of printed, flexible, and/or foldable electronic applications.

■ ASSOCIATED CONTENT

Supporting Information

Detailed experimental procedure, AFM/SEM characterization, thermal gravimetric analysis, ink preparation protocol, printing conditions, and flex testing details. This material is available free of charge via the Internet at http://pubs.acs.org.

■ AUTHOR INFORMATION

Corresponding Author

*E-mail: m-hersam@northwestern.edu.

Author Contributions

The manuscript was written through contributions of all authors. All authors have given approval to the final version of the manuscript.

Notes

The authors declare no competing financial interest.

■ ACKNOWLEDGMENTS

This work was supported by the Office of Naval Research MURI Program (N00014-11-1-0690). A National Science Foundation Graduate Research Fellowship (M.L.G.) is also acknowledged. The authors thank Polyera Corporation (Skokie, IL) for access to their inkjet printing facilities. SEM and AFM characterization was performed in the NUANCE facility at Northwestern University, which is supported by the NSF-NSEC, NSF-MRSEC, Keck Foundation, and State of Illinois.

■ REFERENCES

(1) Arias, A. C.; MacKenzie, J. D.; McCulloch, I.; Rivnay, J.; Salleo, A. Materials and Applications for Large Area Electronics: Solution-Based Approaches. *Chem. Rev.* **2010**, *110*, 3–24.

(2) Sun, J.; Zhang, B.; Katz, H. E. Materials for Printable, Transparent, and Low-Voltage Transistors. *Adv. Funct. Mater.* **2011**, *21*, 29–45.

(3) Kim, D.-H.; Lu, N.; Ma, R.; Kim, Y.-S.; Kim, R.-H.; Wang, S.; Wu, J.; Won, S. M.; Tao, H.; Islam, A.; et al. Epidermal Electronics. *Science* **2011**, *333*, 838–843.

(4) Gaikwad, A. M.; Whiting, G. L.; Steingart, D. A.; Arias, A. C. Highly Flexible, Printed Alkaline Batteries Based on Mesh-Embedded Electrodes. *Adv. Mater.* **2011**, *23*, 3251–3255.

(5) Rogers, J. A.; Bao, Z.; Baldwin, K.; Dodabalapur, A.; Crone, B.; Raju, V. R.; Kuck, V.; Katz, H.; Amundson, K.; Ewing, J.; et al. Paper-Like Electronic Displays: Large-Area Rubber-Stamped Plastic Sheets of Electronics and Microencapsulated Electrophoretic Inks. *Proc. Natl. Acad. Sci. U.S.A.* **2001**, *98*, 4835–4840.

(6) Jung, M.; Kim, J.; Noh, J.; Lim, N.; Lim, C.; Lee, G.; Kim, J.; Kang, H.; Jung, K.; Leonard, A. D.; et al. All-Printed and Roll-to-Roll-Printable Tag on Plastic Foils. *IEEE Trans. Electron Devices* **2010**, *57*, 571–580.

(7) Singh, M.; Haverinen, H. M.; Dhagat, P.; Jabbour, G. E. Inkjet Printing-Process and Its Applications. *Adv. Mater.* **2010**, *22*, 673–685.

(8) Yan, H.; Chen, Z.; Zheng, Y.; Newman, C.; Quinn, J. R.; Dötz, F.; Kastler, M.; Facchetti, A. A High-Mobility Electron-Transporting Polymer for Printed Transistors. *Nature* **2009**, *457*, 679–686.

(9) Hennek, J. W.; Xia, Y.; Everaerts, K.; Hersam, M. C.; Facchetti, A.; Marks, T. J. Reduced Contact Resistance in Inkjet Printed High-

Performance Amorphous Indium Gallium Zinc Oxide Transistors. *ACS Appl. Mater. Interfaces* **2012**, *4*, 1614−1619.
(10) Hoth, C. N.; Choulis, S. A.; Schilinsky, P.; Brabec, C. J. High Photovoltaic Performance of Inkjet Printed Polymer:Fullerene Blends. *Adv. Mater.* **2007**, *19*, 3973−3978.
(11) Hoth, C. N.; Schilinsky, P.; Choulis, S. A.; Brabec, C. J. Printing Highly Efficient Organic Solar Cells. *Nano Lett.* **2008**, *8*, 2806−2813.
(12) Wood, V.; Panzer, M. J.; Chen, J.; Bradley, M. S.; Halpert, J. E.; Bawendi, M. G.; Bulović, V. Inkjet-Printed Quantum Dot−Polymer Composites for Full-Color AC-Driven Displays. *Adv. Mater.* **2009**, *21*, 2151−2155.
(13) Lavery, L. L.; Whiting, G. L.; Arias, A. C. All Ink-Jet Printed Polyfluorene Photosensor for High Illuminance Detection. *Org. Electron.* **2011**, *12*, 682−685.
(14) Dua, V.; Surwade, S. P.; Ammu, S.; Agnihotra, S. R.; Jain, S.; Roberts, K. E.; Park, S.; Ruoff, R. S.; Manohar, S. K. All-Organic Vapor Sensor Using Inkjet-Printed Reduced Graphene Oxide. *Angew. Chem., Int. Ed.* **2010**, *49*, 2154−2157.
(15) Novoselov, K. S.; Fal'ko, V. I.; Colombo, L.; Gellert, P. R.; Schwab, M. G.; Kim, K. A Roadmap for Graphene. *Nature* **2012**, *490*, 192−200.
(16) Kholmanov, I. N.; Magnuson, C. W.; Aliev, A. E.; Li, H.; Zhang, B.; Suk, J. W.; Zhang, L. L.; Peng, E.; Mousavi, S. H.; Khanikaev, A. B.; et al. Improved Electrical Conductivity of Graphene Films Integrated with Metal Nanowires. *Nano Lett.* **2012**, *12*, 5679−5683.
(17) Di, C.; Wei, D.; Yu, G.; Liu, Y.; Guo, Y.; Zhu, D. Patterned Graphene as Source/Drain Electrodes for Bottom-Contact Organic Field-Effect Transistors. *Adv. Mater.* **2008**, *20*, 3289−3293.
(18) Torrisi, F.; Hasan, T.; Wu, W.; Sun, Z.; Lombardo, A.; Kulmala, T. S.; Hsieh, G.-W.; Jung, S.; Bonaccorso, F.; Paul, P. J.; et al. Inkjet-Printed Graphene Electronics. *ACS Nano* **2012**, *6*, 2992−3006.
(19) Lee, S.-K.; Kim, B. J.; Jang, H.; Yoon, S. C.; Lee, C.; Hong, B. H.; Rogers, J. A.; Cho, J. H.; Ahn, J.-H. Stretchable Graphene Transistors with Printed Dielectrics and Gate Electrodes. *Nano Lett.* **2011**, *11*, 4642−4646.
(20) Kim, B. J.; Lee, S.-K.; Kang, M. S.; Ahn, J.-H.; Cho, J. H. Coplanar-Gate Transparent Graphene Transistors and Inverters on Plastic. *ACS Nano* **2012**, *6*, 8646−8651.
(21) Tobjörk, D.; Österbacka, R. Paper Electronics. *Adv. Mater.* **2011**, *23*, 1935−1961.
(22) Li, X.; Cai, W.; An, J.; Kim, S.; Nah, J.; Yang, D.; Piner, R.; Velamakanni, A.; Jung, I.; Tutuc, E.; et al. Large-Area Synthesis of High-Quality and Uniform Graphene Films on Copper Foils. *Science* **2009**, *324*, 1312−1314.
(23) Lin, Y.; Dimitrakopoulos, C.; Jenkins, K. A.; Farmer, D. B.; Chiu, H.; Grill, A.; Avouris, P. 100-GHz Transistors from Wafer-Scale Epitaxial Graphene. *Science* **2010**, *327*, 662.
(24) Li, X.; Zhang, G.; Bai, X.; Sun, X.; Wang, X.; Wang, E.; Dai, H. Highly Conducting Graphene Sheets and Langmuir−Blodgett Films. *Nat. Nanotechnol* **2008**, *3*, 538−542.
(25) Hernandez, Y.; Nicolosi, V.; Lotya, M.; Blighe, F. M.; Sun, Z.; De, S.; McGovern, I. T.; Holland, B.; Byrne, M.; Gun'Ko, Y. K.; et al. High-Yield Production of Graphene by Liquid-Phase Exfoliation of Graphite. *Nat. Nanotechnol.* **2008**, *3*, 563−568.
(26) Eda, G.; Fanchini, G.; Chhowalla, M. Large-Area Ultrathin Films of Reduced Graphene Oxide as a Transparent and Flexible Electronic Material. *Nat. Nanotechnol.* **2008**, *3*, 270−274.
(27) Li, D.; Müller, M. B.; Gilje, S.; Kaner, R. B.; Wallace, G. G. Processable Aqueous Dispersions of Graphene Nanosheets. *Nat. Nanotechnol.* **2008**, *3*, 101−105.
(28) Wang, X.; Zhi, L.; Müllen, K. Transparent, Conductive Graphene Electrodes for Dye-Sensitized Solar Cells. *Nano Lett.* **2008**, *8*, 323−327.
(29) Stankovich, S.; Dikin, D. A.; Dommett, G. H. B.; Kohlhaas, K. M.; Zimney, E. J.; Stach, E. A.; Piner, R. D.; Nguyen, S. T.; Ruoff, R. S. Graphene-Based Composite Materials. *Nature* **2006**, *442*, 282−286.
(30) Lim, S.; Kang, B.; Kwak, D.; Lee, W. H.; Lim, J. A.; Cho, K. Inkjet-Printed Reduced Graphene Oxide/Poly(vinyl alcohol) Composite Electrodes for Flexible Transparent Organic Field-Effect Transistors. *J. Phys. Chem. C* **2012**, *116*, 7520−7525.
(31) Kong, D.; Le, L. T.; Li, Y.; Zunino, J. L.; Lee, W. Temperature-Dependent Electrical Properties of Graphene Inkjet-Printed on Flexible Materials. *Langmuir* **2012**, *28*, 13467−13472.
(32) Shin, K.-Y.; Hong, J.-Y.; Jang, J. Micropatterning of Graphene Sheets by Inkjet Printing and Its Wideband Dipole-Antenna Application. *Adv. Mater.* **2011**, *23*, 2113−2118.
(33) Gómez-Navarro, C.; Weitz, R. T.; Bittner, A. M.; Scolari, M.; Mews, A.; Burghard, M.; Kern, K. Electronic Transport Properties of Individual Chemically Reduced Graphene Oxide Sheets. *Nano Lett.* **2007**, *7*, 3499−3503.
(34) Mattevi, C.; Eda, G.; Agnoli, S.; Miller, S.; Mkhoyan, K. A.; Celik, O.; Mastrogiovanni, D.; Granozzi, G.; Garfunkel, E.; Chhowalla, M. Evolution of Electrical, Chemical, and Structural Properties of Transparent and Conducting Chemically Derived Graphene Thin Films. *Adv. Funct. Mater.* **2009**, *19*, 2577−2583.
(35) Hernandez, Y.; Lotya, M.; Rickard, D.; Bergin, S. D.; Coleman, J. N. Measurement of Multicomponent Solubility Parameters for Graphene Facilitates Solvent Discovery. *Langmuir* **2010**, *26*, 3208−3213.
(36) Behabtu, N.; Lomeda, J. R.; Green, M. J.; Higginbotham, A. L.; Sinitskii, A.; Kosynkin, D. V; Tsentalovich, D.; Parra-Vasquez, A. N. G.; Schmidt, J.; Kesselman, E.; et al. Spontaneous High-Concentration Dispersions and Liquid Crystals of Graphene. *Nat. Nanotechnol.* **2010**, *5*, 406−411.
(37) Green, A. A.; Hersam, M. C. Solution Phase Production of Graphene with Controlled Thickness via Density Differentiation. *Nano Lett.* **2009**, *9*, 4031−4036.
(38) Liang, Y. T.; Hersam, M. C. Highly Concentrated Graphene Solutions via Polymer Enhanced Solvent Exfoliation and Iterative Solvent Exchange. *J. Am. Chem. Soc.* **2010**, *132*, 17661−17663.
(39) Seo, J. T.; Green, A. A.; Antaris, A. L.; Hersam, M. C.; Copolymers, B. B. High-Concentration Aqueous Dispersions of Graphene Using Nonionic, Biocompatible Block Copolymers. *J. Phys. Chem. Lett.* **2011**, *2*, 1004−1008.
(40) Lotya, M.; Hernandez, Y.; King, P. J.; Smith, R. J.; Nicolosi, V.; Karlsson, L. S.; Blighe, F. M.; De, S.; Wang, Z.; McGovern, I. T.; et al. Liquid Phase Production of Graphene by Exfoliation of Graphite in Surfactant/Water Solutions. *J. Am. Chem. Soc.* **2009**, *131*, 3611−3620.
(41) Soltman, D.; Subramanian, V. Inkjet-Printed Line Morphologies and Temperature Control of the Coffee Ring Effect. *Langmuir* **2008**, *24*, 2224−2231.
(42) De Gans, B.-J.; Schubert, U. S. Inkjet Printing of Well-Defined Polymer Dots and Arrays. *Langmuir* **2004**, *20*, 7789−7793.
(43) Jeong, S.; Kim, D.; Moon, J. Ink-Jet-Printed Organic−Inorganic Hybrid Dielectrics for Organic Thin-Film Transistors. *J. Phys. Chem. C* **2008**, *112*, 5245−5249.
(44) Lim, J. A.; Lee, W. H.; Lee, H. S.; Lee, J. H.; Park, Y. D.; Cho, K. Self-Organization of Ink-Jet-Printed Triisopropylsilylethynyl Pentacene via Evaporation-Induced Flows in a Drying Droplet. *Adv. Funct. Mater.* **2008**, *18*, 229−234.
(45) Hu, H.; Larson, R. G. Marangoni Effect Reverses Coffee-Ring Depositions. *J. Phys. Chem. B* **2006**, *110*, 7090−7094.
(46) Keiluweit, M.; Nico, P. S.; Johnson, M. G.; Kleber, M. Dynamic Molecular Structure of Plant Biomass-Derived Black Carbon (Biochar). *Environ. Sci. Technol.* **2010**, *44*, 1247−1253.
(47) Pastorova, I.; Botto, R. E.; Arisz, P. W. Cellulose Char Structure: A Combined Analytical Py-GC-MS, FTIR, and NMR Study. *Carbohydr. Res.* **1994**, *262*, 27−47.